Characterization and correction of evaporative artefacts in speleothem fluid inclusion isotope analyses as applied to a stalagmite from Borneo.

A. Fernandez[1,2,3], M. H. Løland[1,3]., J. Maccali[1,3,4], Y. Krüger[1], H.B. Vonhof[5], H. Sodemann[3,6], A. N. Meckler[1,3,4]

[1]Department of Earth Sciences, University of Bergen, Bergen, Norway
[2]Andalusian Institute of Earth Sciences, CSIC-University of Granada, Granada, Spain
[3]Bjerknes Centre for Climate Research, Bergen, Norway
[4]SFF Centre for Early Sapiens Behaviour (SapienCE), University of Bergen, Bergen, Norway
[5]Max Planck Institute for Chemistry, Climate Geochemistry Department, Mainz, Germany
[6]Geophysical Institute, University of Bergen, Bergen, Norway

Abstract

Fluid inclusion water isotope measurements in speleothems have great potential for paleoclimate studies, as they can be used to provide reconstructions of precipitation dynamics and land temperature. Several previous observations, however, suggest that inclusion waters do not always reflect the isotopic composition of surface precipitation. In such cases, dripwaters are thought to be modified by evaporation in the cave environment that result in more positive δ^2H and $\delta^{18}O$ values and shallow $\delta^2H/\delta^{18}O$ slopes. Although evaporation can occur in cave systems, water can also be lost to evaporation during analysis but before water extraction. Here, we examine the likelihood of this possibility with a stalagmite from Borneo. We demonstrate that many samples loose water, and that water loss is controlled by the type and size of inclusions. With multiple replicate measurements of coeval samples, we calculate an evaporative $\delta^2H/\delta^{18}O$ slope of 1±0.6 (2SE). This value is consistent with model predictions of evaporative fractionation at high analytical temperature at low humidity. Finally, we provide a robust and physically based correction method. We find that fluid–calcite $\delta^{18}O$ paleotemperatures calculated with corrected $\delta^{18}O$ data show excellent agreement with recent microthermometry temperature estimates for Borneo during the last deglaciation, suggesting minimal variations in stalagmite $\delta^{18}O$ disequilibrium over time. Similarly, corrected fluid inclusion $\delta^{18}O$ and δ^2H values follow the expected hydroclimate response of Borneo to periods of reduced Atlantic Ocean meridional overturning circulation. Our results suggest that careful petrographic examination and multiple replicate measurements are necessary for reliable paleoclimate reconstructions with speleothem fluid inclusion water isotopes.

1.0 Introduction

The majority of stalagmite-derived paleoclimate reconstructions have traditionally been based on the oxygen isotope composition of carbonate (e.g., Fleitmann et al., 2003; Wang et al., 2001). More recently, thanks to recent technological improvements (e.g., Affolter et al., 2014; Dassié et al., 2018; de Graaf et al., 2020), research has increasingly focused on

measurements of fluid inclusion water isotopes. Fluid inclusions in speleothems preserve relics of ancient dripwater. Measurements of δ^2H and $\delta^{18}O$ in fluid inclusion water offer unique advantages relative to carbonate $\delta^{18}O$ values alone. They provide a more direct constraint on rainwater $\delta^{18}O$ than carbonate $\delta^{18}O$. Thus, they can be used to reconstruct changes in precipitation dynamics such as rainfall amounts (e.g., Arienzo et al., 2015; van Breukelen et al., 2008; Millo, 2017) and in the sources of moisture (e.g., Matthews et al., 2021; Rogerson et al., 2019), especially when supported by suitable moisture transport information (e.g., Baker et al., 2015). They also allow disentangling the respective contributions of temperature and dripwater $\delta^{18}O$ variability on stalagmite carbonate $\delta^{18}O$ (e.g., Arienzo et al., 2015; Meckler et al., 2015, 2021; Wortham et al., 2022), yielding temperature estimates from the difference of $\delta^{18}O$ in inclusion water and the surrounding calcite . Additionally, in settings where temperature is the main control on rainfall isotope variability, fluid inclusion measurements have also been used directly to estimate air temperature at the site of precipitation, assuming that present-day relationships hold true for the past (Affolter et al., 2019).

Fluid inclusions often yield meaningful isotope values showing that the isotopic composition of the inclusion water is well preserved. Fluid inclusion isotope analyses thus contribute significantly to our understanding of speleothem paleoclimate records. However, observations from some stalagmites suggest that recovery of the original isotope signal of precipitation is not always possible. For instance, recently published fluid inclusion isotope data from five stalagmites show large positive enrichments in δ^2H and $\delta^{18}O$ values that in some cases plot far to the right of local meteoric water lines (LMWLs) (Affolter et al., 2019; Matthews et al., 2021; Nehme et al., 2020; Warken et al., 2022; Wortham et al., 2022). These data are usually obtained from samples with relatively low water yields, and follow typical evaporation lines in a $\delta^2H/\delta^{18}O$ diagram. Such observations suggest that fluid inclusion waters can be modified to an extent that they no longer reflect the isotopic composition of surface precipitation. Modification of fluid inclusion water $\delta^{18}O$ through carbonate-water isotope exchange has been proposed (Demény et al., 2016), but fails to explain the enrichment observed in both δ^2H and $\delta^{18}O$ values. Additionally, such O isotope exchange has been shown not to readily occur in speleothems (Uemura et al., 2019).

A common hypothesis to explain the mismatch between LMWLs and the fluid inclusion isotopes is that modifications are the result of evaporative fractionation in the soil, epikarst, or cave environment. Evaporation results in heavier oxygen and hydrogen isotope compositions relative to the initial liquid and in shallow $\delta^2H/\delta^{18}O$ slopes that intersect the steeper local meteoric water lines (LMWLs) (e.g., Craig H, 1961; Horita et al., 2008). While this hypothesis appears at first sight to explain the main observations outlined above, there are other possible explanations. Several studies have raised the possibility that evaporation could also occur during analysis when samples are placed in an analytical apparatus at high temperatures (typically 120°C; Matthews et al., 2021; Warken et al., 2021). However, additional data from experiments and measurements of natural samples are needed to determine which of the hypotheses explains the observations.

Here, we test the reliability of fluid inclusion isotope analyses with a stalagmite from Borneo that grew during the last deglaciation. We specifically examine the extent to which fluid inclusion waters can evaporate during laboratory analyses before the crushing step that releases water to the analyzer. Borneo is the ideal location for this work for several reasons. Evaporation in Borneo caves is unlikely given the year-round 100% relative humidity of cave air at this tropical location (Meckler et al., 2015). If isotopic enrichments occur in fluid inclusion water isotopes, they are most likely the result of another process. Furthermore, the temperature and hydroclimate evolution of Borneo through the deglaciation are relatively well understood. Changes in hydroclimate are constrained with carbonate $\delta^{18}O$ measurements, which reproduce well across four different stalagmites (Buckingham et al., 2022; Partin et al., 2007), suggesting minimal variations over time in isotopic disequilibrium during stalagmite formation. The interpretation of carbonate $\delta^{18}O$ is corroborated by calculated drip-water $\delta^{18}O$ values (Løland et al., 2022), and is consistent with isotope-enabled transient climate simulations (Buckingham et al., 2022; He et al., 2021). The regional temperature evolution is well-constrained with fluid inclusion microthermometry, a method that produces exceptionally precise paleotemperatures (Krüger et al., 2011). These available constraints allow us to compare fluid inclusion water isotope data to independently derived dripwater $\delta^{18}O$, and calculated fluid-calcite $\delta^{18}O$ temperatures with available microthermometry estimates.

2.0 Methods

2.1 Site and sample description

We measured water isotopes in fluid inclusions (also referred to as fluid inclusion isotopes here) from a stalagmite collected in Northern Borneo (SSC01; Partin et al. 2007). Borneo is located in the tropical West Pacific, the region with the warmest modern ocean temperatures. The site remains year-round within the center of tropical convection as the Intertropical Convergence Zone (ITCZ) migrates north and south. The region receives an average of 5000 mm annual rainfall with only weak seasonality. The stalagmite SSC01 was collected in 2003 from Snail Shell Cave (4º 12’ 20.8” N, 114 º 56’26.9” E), which is located in Gunung Buda in the northwestern corner of Malaysian Borneo and has previously been dated and investigated for carbonate $\delta^{18}O$ (Partin et al., 2007).

We compare our data to calculated dripwater isotope values and fluid inclusion microthermometry estimates from another stalagmite from an adjacent mountain, SC02 (Løland et al., 2022). Stalagmite SC02 was collected in 2006 from Secret Chamber in Gunung Mulu National Park (Buckingham et al., 2022). Dripwater isotope values in Gunung Mulu caves have been shown to closely match rainfall $\delta^{2}H$ and $\delta^{18}O$ values with an average residence time in the karst of 3 to 18 months, and regional rainfall amount is thought to exert the dominant control on interannual rainfall isotope variability (Ellis et al., 2020; Moerman et al., 2014). The position of the local meteoric water line (LMWL) is well constrained with quasi biweekly dripwater samples collected from 2006 to 2018 at three sites in two caves (see supplemental

1). A linear regression drawn through these data results in the following equation: $\delta^2H = 8.06\ (\pm 0.04) \times \delta^{18}O + 13.74\ (\pm 0.3)$. Long multi-year measurements of cave temperatures exist for several caves in Gunung Mulu, and these show that cave temperatures remain close to 24°C with less than 0.2 °C variations throughout the year (Løland et al., 2022). Since long-term temperature measurements do not exist for Snail Shell Cave, we assume that the nearby Mulu temperature range is also representative for that site.

The SSC01 stalagmite was originally split in half along the central growth axis by Partin et al. (2007), who used one half for geochemical analyses, while the other half is used here. The stalagmite half was embedded in plaster, and a diamond wire saw (Well 6500) was used to cut slabs of 7 mm thickness lengthwise. Blocks of 20 to 40 mm length and 20 mm width were then cut from the slabs along the central axis. Before the blocks were sampled for fluid inclusion isotope analyses, thin sections were obtained for petrographic inspection. Samples for fluid inclusion analysis were then cut from the blocks with a smaller diamond wire saw (Well 3421). To this end, the calcite blocks were first glued to glass plates on both sides and fixed on the sample holder of the saw. The sample holder was attached to a translation stage, which enables stepwise lateral displacement of the sample with respect to the cutting direction resulting in a curvature of the cuts. The samples were cut along to the growth bands closely following their three-dimensional orientation. This ensures that coeval samples are obtained. Two to five samples were obtained from each block and placed in acetone to remove the glued glass plates. These samples were then cut into three to four equally sized replicate samples of approximately 0.2 to 0.8 g.

2.2 Calcite stable isotope measurements and age model

To place the results in the revised chronology of (Partin, 2008), calcite $\delta^{18}O$ was re-measured on the sample blocks and the results were compared to the published record (Supplemental 2). Samples were obtained by continuous milling at 1 mm increments with a Sherline 540 micromill. Measurements were performed in the Facility for Advanced Isotopic Research (FARLAB) at the Department of Earth Science at the University of Bergen using a MAT 253 isotope ratio mass spectrometer (IRMS-Thermo Fisher) coupled to a Kiel IV carbonate preparation device. A total of 347 calcite samples were measured. The average measurement error is less than 0.05‰ (1σ) for $\delta^{13}C$ and 0.10‰ (1σ) for $\delta^{18}O$.

2.3 Fluid inclusion isotope measurements

Fluid inclusion water isotope measurements were conducted following the procedures described by de Graff et al. (2020). The analytical line consists of a crusher device that is connected to a humidity generator and to a Picarro cavity ring-down spectrometer (CRDS) on opposite ends. The crusher device is constructed in stainless steel and follows the design of de Graff et al. (2020) with some modifications. Samples were measured with all analytical components under constant humid conditions to avoid memory effects (Affolter et al., 2014; Dassié et al., 2018; de Graaf et al., 2020). The humidity generator is composed of a modified 300 ml stainless-steel cylinder that serves as an evaporation chamber and a microdrop

dispenser head (MK-130, Microdrop GmbH, Germany) that ejects water droplets (<100 µm diameter) into the evaporation chamber by piezoelectric stimulation. Specific details on the design and performance of the humidity generator device are described in Sodemann et al. (in prep). During analyses the evaporation chamber of the humidity generator was kept at a constant temperature of 60°C. The crusher device and related stainless-steel lines were kept at a temperature of 120°C. A distilled water standard of known isotopic composition (DI2; $\delta^{18}O$ = -7.63 ± 0.06 and $\delta^{2}H$ = -50.72 ± 0.46) was used to generate the humid background.

Depending on the expected water content, between 0.2 to 0.8 g of stalagmite sample were used for analyses, and whenever possible samples were measured a minimum of three times. A total of 119 replicate analyses from 40 samples were performed. Before analysis, samples were loaded into the pre-heated crusher device and approximately 15-25 minutes were needed for background stabilization. After stabilization the sample was crushed, and the resulting water was measured by the analyzer. Raw $\delta^{18}O$ and $\delta^{2}H$ data for sample and background were corrected for the humidity dependency of the analyzer following the procedures described in (Weng et al., 2019). Sample $\delta^{18}O$ and $\delta^{2}H$ values were then calculated following the algorithm presented by Affolter et al. (2014). These were subsequently normalized to the VSMOW scale with a set of three in-house water standards, which had previously been calibrated against international standards. Standards were injected on a daily basis through a port that is installed immediately before the crusher device. The analytical precision (1σ) of replicate analyses for samples larger than 0.3 µl, as judged by injected calibration standards, are 0.3‰ and 1.3 ‰ for $\delta^{18}O$ and $\delta^{2}H$, respectively. For samples between 0.1 and 0.3 µl, precisions are 0.4‰ and 1.4 ‰ for $\delta^{18}O$ and $\delta^{2}H$. Final errors in fluid inclusion data are presented as confidence intervals at 68 or 95%. These are calculated with the standard deviation of replicate analyses or the long-term reproducibility from water standards (shown above), whichever was greater.

The accuracy of water isotope measurements with the crushing line was assessed with standard waters sealed in borosilicate glass capillaries (following Weißbach, 2020), and with aliquots of a travertine sample that was previously measured in another laboratory (Semproniano travertine, de Graaf et al. 2020) The glass capillary samples were designed to mimic real inclusions since they receive the same treatment as calcite samples (i.e., water is released in the same location as calcite samples by turning the thread of the crusher device). The mean values obtained for both glass capillaries and the travertine are statistically indistinguishable from their 'known' values. Stalagmite water amounts (µl/g) were calculated with a transfer function built with calculated water amounts (area under peaks) and water amounts from injections of standard waters (0.05-1 µl, r^2=0.99, RMSE=0.02). The accuracy of water amount measurements were determined to be ± 5% (1σ) based on weighted glass capillaries.

3 Results

3.1 Petrography – SSC01 Calcite Fabrics and Fluid Inclusions

Thick sections (200 µm) of stalagmite SSC01 were investigated with an optical microscope under plane polarized (PPL) and cross polarized light (XPL) to characterize the calcite fabrics and occurrence of fluid inclusions. The calcite fabrics and occurrence of fluid inclusions can be classified into two general groups that are closely associated with age. For instance, Holocene and late deglacial calcite fabrics are dominated by clear, transparent columnar calcite with straight crystal boundaries and up to centimeter wide domains of uniform extinction under XPL (Figure 1A ,1B). The fabric is characterized by countless very small fluid inclusions that are dispersed in the matrix and range in size between 1 and 10 µm^3 (Figure 1C), and by some large up to 1 mm long inter-crystalline inclusions. Sporadically, the calcite fabric is interrupted by distinct layers with numerous inclusions in the range of 10^2- 10^3 µm^3 (Fig. 1A, 1B). These inclusion-rich layers possibly formed onto former growth hiatuses. Early deglacial and glacial samples, in contrast, consist of alternating layers of open columnar and microcrystalline calcite fabrics (Figure 1C, 1D). The latter are rich in organic matter, as confirmed by confocal fluorescence microscopy. Fluid inclusions are abundant in the columnar fabric and orders of magnitudes larger (10^3 and 10^5 µm^3) than the tiny inclusions that dominate the main part of the Holocene and late deglacial fabric of stalagmite SSC01 (Figure 1F). Large inter-crystalline inclusions are also present in the early deglacial and glacial parts of the stalagmite.

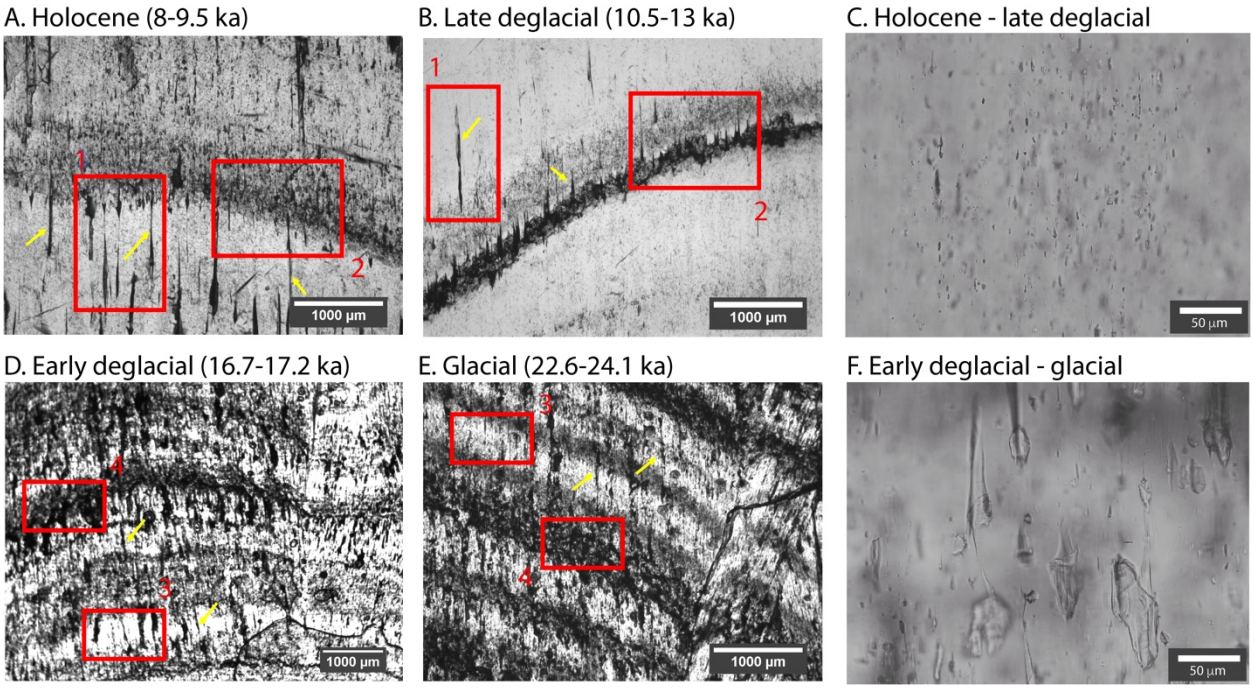

Figure 1. Optical microphotographs of polished thick sections from representative portions of the glacial, deglacial, and Holocene sections of SSC01. A and B) thin section images from Holocene and late deglacial sections taken under cross-polarized light. C) microphotograph at higher magnification showing the very small (1 and 10 µm^3) inclusions present in the Holocene and late deglacial portions of the stalagmite. 1) columnar calcite with countless tiny fluid inclusions and some large inter-crystalline inclusions indicated by yellow arrows. 2) dark inclusions-rich layers possibly overgrowing a former hiatus surface enriched in organic material. D and E) thin section images from the early deglacial and the glacial portion of the stalagmite taken under cross-polarized light. F) microphotograph at higher magnification showing the large (10^3 and 10^5 µm^3) inclusions present in the early deglacial and glacial portions of the stalagmite. 3) example of light, transparent open columnar layers with abundant large fluid inclusions. 4) examples of dark-colored layers composed of organic-rich microcrystalline calcite. Yellow arrows indicate large elongated inter-crystalline fluid inclusions.

3.2 Relationship of fluid inclusion isotope data to the LMWL

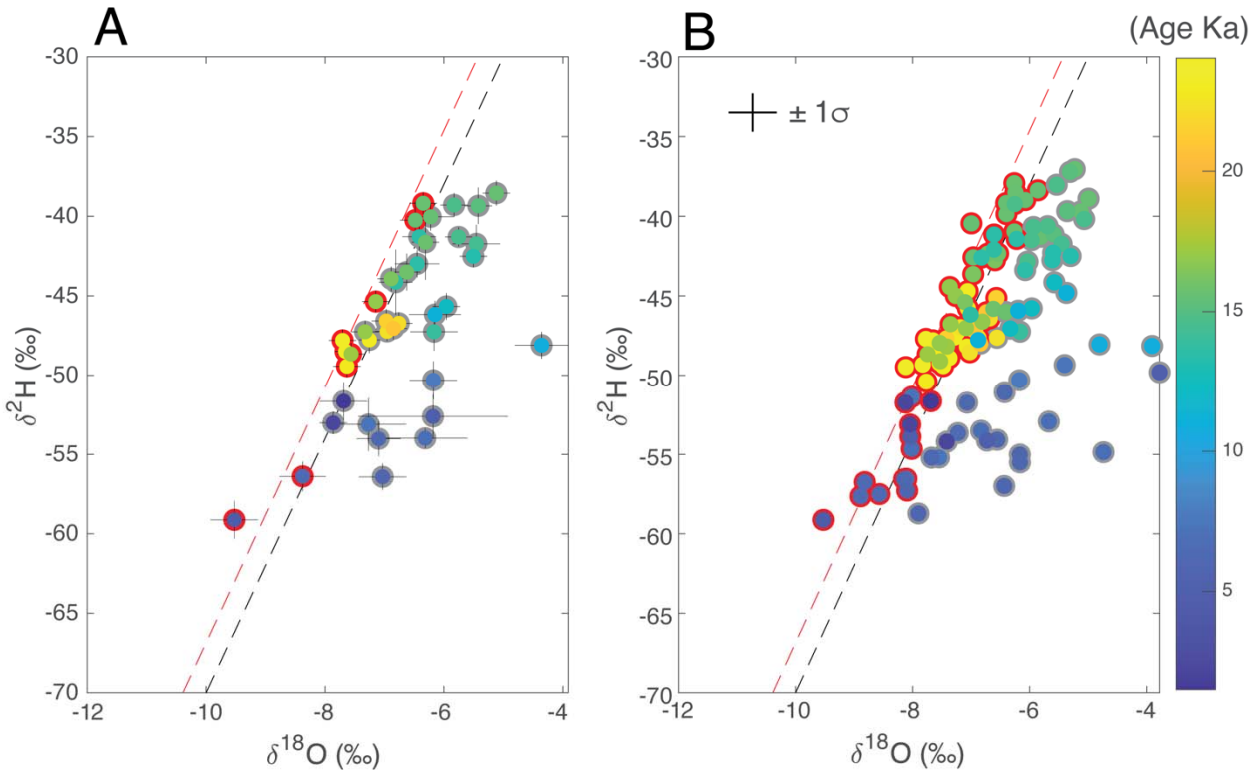

Figure 2. Fluid inclusion water isotope composition. A) Plot of sample means. B) Plot of replicate analyses. Points with red borders are within ± 68% (CI) of the LMWL. Data points are color coded by age as shown in the colorbar. The red dashed line is the LWML and black dashed line is the global meteoric water line (GMWL). Error bars in A and B are 68% confidence intervals.

A cross-plot of the stalagmite fluid inclusion water isotope data shows that the majority of samples (31 out of 40, i.e. 78%) have values that are outside 1σ (68% CI) analytical uncertainty of the local meteoric water line (LMWL; Figure 2A). Moreover, many data points are systematically shifted towards more positive $\delta^{18}O$ values with only small changes present in $\delta^{2}H$ values. This is most clearly seen in Figure 2B where we present individual replicate analyses. We observe that replicate analyses do not fall randomly off the LMWL. They instead follow linear trends with shallow slopes that intersect the LMWL (Fig. 3). To investigate the cause for the observed deviations from the LMWL, we calculated the slopes in $\delta^{2}H$ -$\delta^{18}O$ for samples with three or more replicate measurements, and where the standard deviation in $\delta^{18}O$ values was larger than 0.4 ‰ (i.e., the long-term analytical reproducibility; Fig. 3A). This last step is necessary because many data points are within error of each other, and a larger spread in $\delta^{18}O$ values allows for a more accurate slope determination. Eleven samples met these criteria, and we obtained an average value of 1 ± 0.6 (2 SE) for the slopes among their replicate results (see Supplemental 3 for details). Moreover, we observe a general relationship between $\delta^{18}O$ deviations from the LMWL ($\Delta\delta^{18}O$ LMWL) and the amount of water that was recovered during its analysis (i.e., less water was obtained from replicates that are further away from the LMWL). This is true for 9 out of the 11 samples that we considered, as can be seen by the negative slopes in water content (µl/g) vs. $\Delta\delta^{18}O$ LMWL (‰) in Figure 3B.

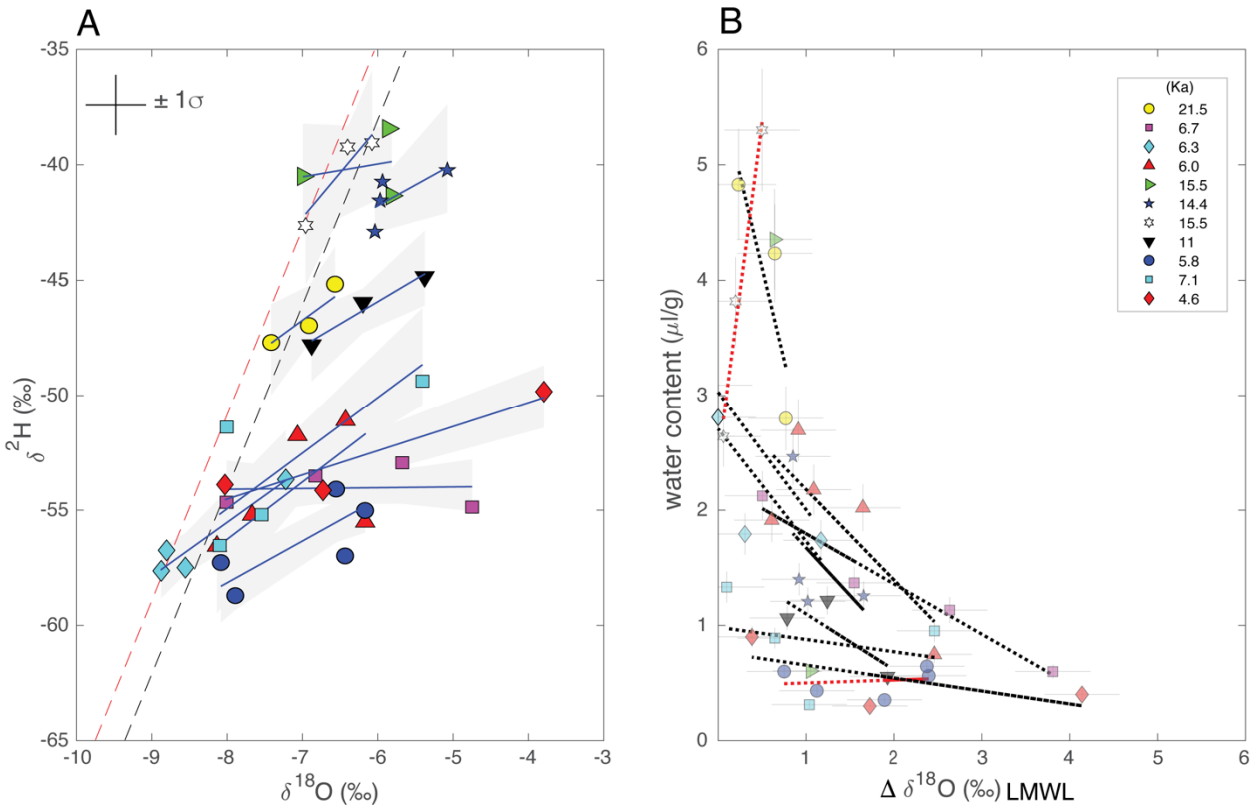

Figure 3. A) Linear regressions through replicate water isotope measurements. Each color and symbol combination represents one sample (11 samples total). Only samples with three or more replicates and

standard deviations in $\delta^{18}O$ greater than 0.4 ‰ are shown. Blue lines are individual linear fits calculated with the algorithm of York et al. (2004). Shaded grey regions are regression 68% confidence intervals obtained by Monte Carlo simulations considering errors in both $\delta^{18}O$ and $\delta^{2}H$ values. B) Water content of individual replicate analyses vs. $\Delta\delta^{18}O$ LMWL ($\delta^{18}O$ deviation from LMWL). Black dashed lines are linear regressions with negative slopes, and red dashed lined are linear regressions with positive slopes.

3.2 – Relationships between fluid inclusions, water content and $\delta^{18}O$ deviations from the LMWL

There is a close association between water content, $\delta^{18}O$ deviations from the LMWL ($\Delta\delta^{18}O$ LMWL), and the occurrence of fluid inclusions in the stalagmite. Higher water contents are observed in samples from the early deglacial and glacial samples (Figure 4A); these samples have abundant large (i.e., 10^3 and 10^5 μm^3) fluid inclusions in the open columnar fabric. Much lower water amounts were observed in the Holocene and late deglacial samples (Figure 4A). These samples have abundant but small inclusions (i.e., 1 and 10 μm^3) and very few larger (i.e., up to 1 mm long) inter-crystalline inclusions. The abrupt change in water content that we observe during the deglaciation is also mirrored in the proportions of samples and replicate analyses that fall off the LWML (Figure 4B). For instance, most of early deglacial and LGM samples fall close to the LMWL, i.e., they have $\delta^{18}O$ values that are close to what is expected based on their $\delta^{2}H$ composition ($\Delta\delta^{18}O$ LMWL values are close to zero). The younger samples from the late deglacial and Holocene, however, have $\delta^{18}O$ values that, with few exceptions, fall off the LMWL and are farther away from the LWML.

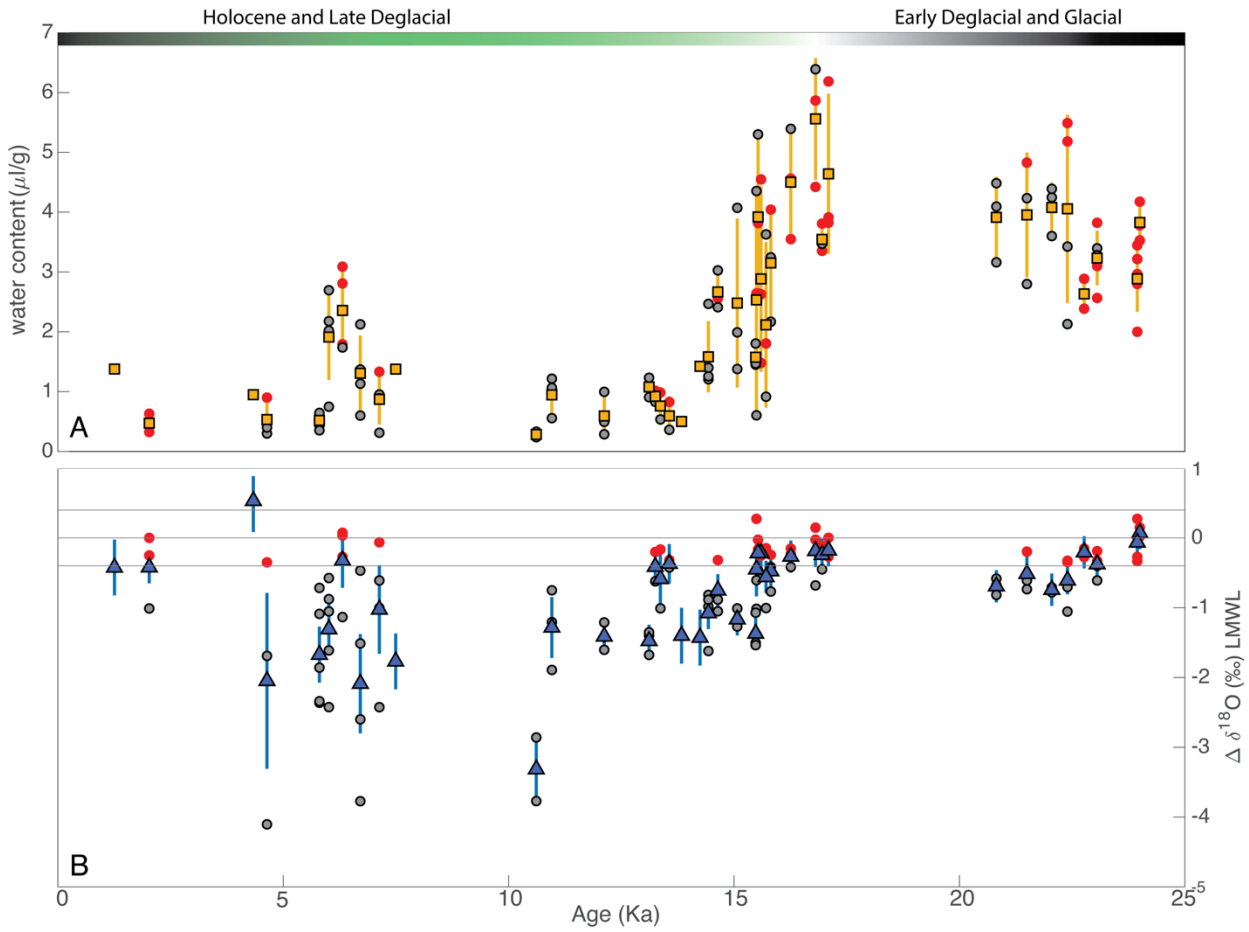

Figure 4. A) Water content (µl/g) of SSC01 stalagmite plotted against age. Yellow squares are mean values of replicate analyses, and circles are individual analyses. Red circles are replicates with $\delta^{18}O$ and $\delta^{2}H$ values that fall within 68% CI of the LMWL. B) $\delta^{18}O$ deviations from the LMWL ($\Delta\delta^{18}O$ LMWL). Circles are replicate analyses and blue triangles are sample means. Red data circles are replicates that have values that fall on the LMWL.

3.2 Comparison of inclusion data with independent temperature and dripwater $\delta^{18}O$ proxies

The time-dependence of observed offsets and their possible cause can be further investigated by comparing the fluid inclusion isotope results to available independent information on temperature (from fluid inclusion microthermometry; Løland et al., 2022) and dripwater $\delta^{18}O$ from stalagmite SC02 collected from a cave in an adjacent mountain (Fig 5). Dripwater $\delta^{18}O$ values for SC02 were calculated with microthermometry temperature estimates and the corresponding calcite $\delta^{18}O$ values using the empirical cave calibration for $\delta^{18}O$ of Tremaine et al. (2011) (see Løland et al., 2022). We observe that SSC01 fluid inclusion $\delta^{18}O$ values are generally more positive than calculated drip water values from SC02. However, values are closer to those in SC02 in older parts of the SSC01 record than in younger parts. Moreover, we find closer agreement when only the SSC01 $\delta^{18}O$ values that fall on the LMWL are

considered (Figure 5A). The agreement is even more apparent when only individual replicate analyses are considered; replicates that fall on the LMWL follow the same trends as in SC02 throughout the length of the record (Supplementary Figure 4). In contrast to fluid inclusion $\delta^{18}O$, $\delta^{2}H$ values are much closer to the calculated SC02 drip water values, although still showing larger deviations in the younger part of the record (Figure 5B).

If we were to use our fluid inclusion water isotope results at face value, fluid-calcite $\delta^{18}O$ temperatures, calculated with the equation of Tremaine et al. (2011), yield mostly unrealistically high temperatures and are almost always warmer than microthermometry estimates (Figure 5C). A closer agreement is observed during the LGM and the early deglacial where temperatures are on average 2.3°C degrees warmer. In younger samples, on the other hand, temperatures are on average 7.3°C warmer than fluid inclusion homogenization temperatures. In a similar manner to SSC01 fluid inclusion $\delta^{18}O$ values, we observe better agreement between both paleothermometers when only temperatures calculated with $\delta^{18}O$ values that fall on the LMWL are considered. This is true at the sample mean and the replicate level (Figure 5C and Supplemental 4). Overall, the comparison with independent constraints supports our interpretation that the offsets from the LMWL are likely artifacts and illustrates their impact on the interpretation of the results.

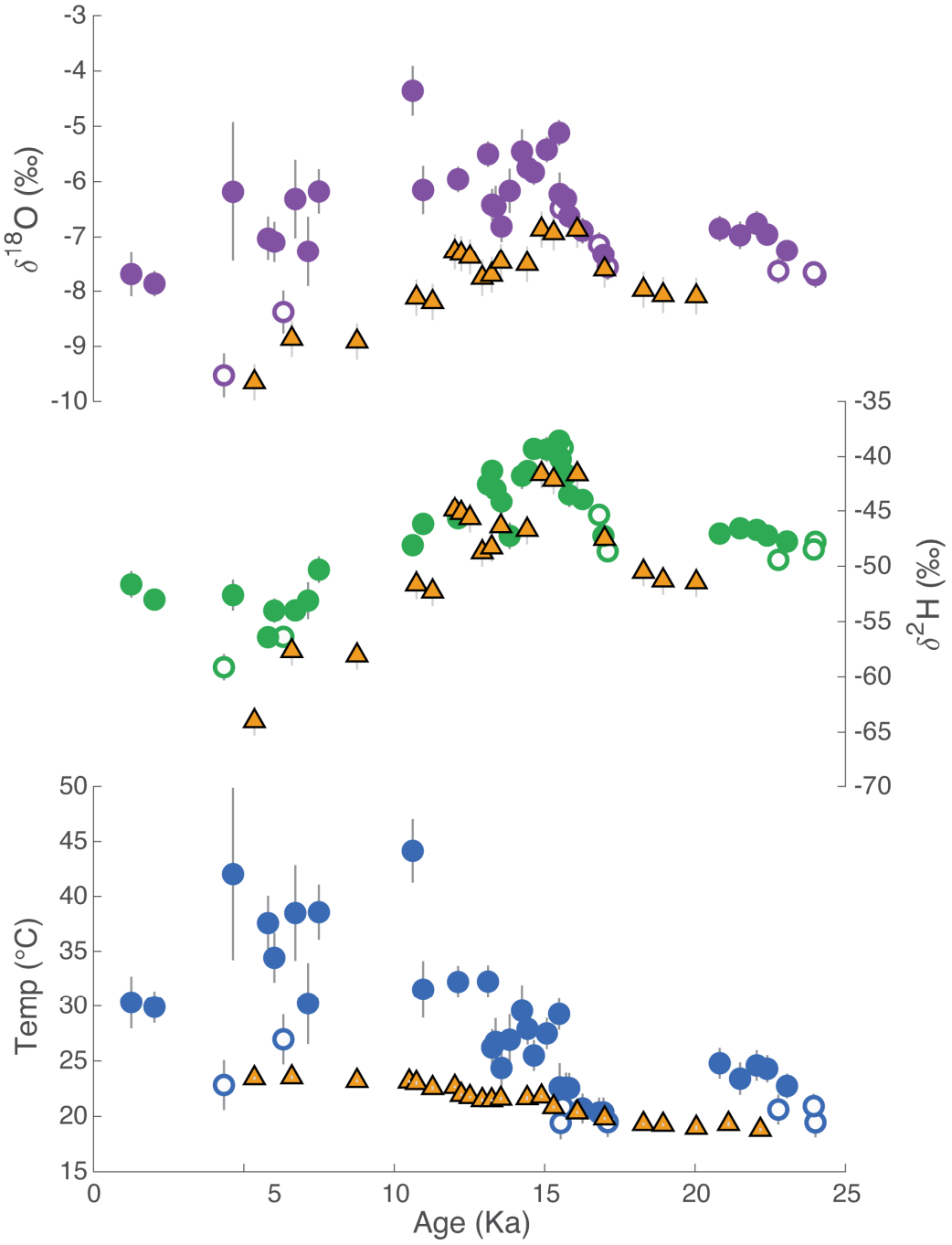

Figure 5. A) Measured fluid inclusion $\delta^{18}O$ values of stalagmite SSC01 (circles) and calculated drip water $\delta^{18}O$ values of stalagmite SC02 from the same region (triangles; Løland et al., 2022). B) Measured fluid inclusion $\delta^{2}H$ values of SSC01 (circles) and calculated drip water $\delta^{2}H$ values of SC02, using the LMWL (triangles). C) fluid-calcite $\delta^{18}O$ temperatures of SSC01 calculated with the temperature relationship of Tremaine et al. (2011) (circles) and fluid inclusion microthermometry temperatures of SC02 from Løland et al. (2021). Error bars are 68% confidence intervals. Open circles are samples that fall within 68% CI of the LMWL.

4. Discussion

4.1 Water loss through evaporation during analyses

We observe enrichments in fluid inclusion δ^2H and $\delta^{18}O$ values, shallow $\delta^2H/\delta^{18}O$ slopes in replicate analyses, and poor agreement between fluid inclusion data and independent paleoclimate proxies. These observations could be interpreted as indication of evaporation in the cave. For the cave site investigated here, however, we expect that evaporation inside the cave is unlikely given a year-round relative humidity in Borneo caves of nearly 100% (Meckler et al., 2015). For this reason, we now explore the alternative hypothesis that evaporation occurred in the crusher device at 120 ˚C, immediately before the crushing step. The physical reasoning behind this hypothesis is the increase of fluid pressure with increasing temperature in an isochoric system. At a certain threshold the fluid overpressure inevitably induces irreversible volume changes of the inclusions, most likely due to the formation of cracks in the confining calcite host, preferentially along the cleavage planes and, in case of inter-crystalline inclusions, along crystal boundaries. The formation of cracks results in a volume increase of the inclusions, and thus, in a relaxation of the fluid overpressure. Upon further heating, the cracks propagate and waters can then leak along crystal boundaries, internal porosity and primary fractures in the stalagmite and evaporate. Partial evaporation of water from fluid inclusions would then lead to some degree of isotopic modifications and enrichments in δ^2H and $\delta^{18}O$ values and thus affect the isotope signal that is measured after crushing the sample. Inclusions that lose all their water in the course of the 15-20 minutes of background stabilization, on the other hand, have no effect on the measured isotope signal.

Ideally water loss can be observed as samples are heated and the evolving water is detected by the analyzer. However, this is not possible with our analytical set-up. When the crusher device is opened to load a sample, the water background measured by the analyzer quickly decreases to match the humidity of the laboratory air. Once the crusher is closed, the humidity slowly rises over the next 15-20 minutes to the level set by the humidity generator. This makes it impossible to observe any water loss from the sample that may be occurring during this time. For that reason, we designed an experiment to manometrically determine if water is lost as a sample is heated in a vacuum line (see supplemental 5 for details). Briefly, a sample was loaded into a glass tube, connected to a vacuum line and evacuated. The sample was then heated to approximately 120°C with a heat gun, and any released water was collected in a cold trap bathed in liquid N_2. After 20 minutes, the liquid N_2 was removed, and the water pressure was measured in a manometer. The manometer pressure was calibrated for water amounts by adding known amounts of water to the same volume. The experiment was performed with two different samples from the Holocene portion of the stalagmite; we estimate that for both samples approximately 10% of the water content was lost (see supplemental 5 for details).

4.2 Evaporation model

We have demonstrated that in our samples, water loss can occur at temperatures of 120°C, and have argued that sample specific evaporative trends are suggestive of analytical artifacts. In the next section, we use a Rayleigh model to simulate the isotopic composition of water during fluid inclusion analysis, in comparison to those that would be expected for evaporation in cave environments. These predictions are then used to determine if the $\delta^2H/\delta^{18}O$ slopes and the magnitudes of isotopic fractionations observed in the fluid inclusion data are characteristic of the temperature and humidity conditions of the crusher device.

Isotope ratios during evaporation can be calculated with the Rayleigh equation:

$$R_l = R_{l-0} \times f^{(\alpha_{eff}-1)} \qquad (1)$$

where R_l is the isotope ratio (^{18}R or ^{2}R) of the liquid at each step of an evaporative process, R_{l-0} is the isotope ratio of the initial liquid, f is the fraction of liquid remaining at each step, and α_{eff} is the effective vapor-liquid isotope fractionation factor during evaporation ($R_v/R_l < 1$). α_{eff} was calculated with the formulation of the Craig-Gordon model (Craig and Gordon, 1965) for evaporation into an atmosphere of fixed humidity and isotopic composition:

$$\alpha_{eff} = \alpha_{diff} \left[\frac{\alpha_{eq} - h(R_a/R_l)}{1-h}\right] \qquad (2)$$

where α_{eq} is the temperature dependent equilibrium vapor-liquid isotope fractionation factor, h is the relative humidity, R_a is the isotope ratio in air, R_l is the isotope ratio in the liquid, and α_{diff} is the isotope fractionation during diffusion in air. α_{diff} can be expressed as the ratio of the molecular diffusivities of the heavy (HDO and $H_2{}^{18}O$) and light (H_2O and $H_2{}^{16}O$) water isotopologues:

$$\alpha_{diff} = \left(\frac{D_H}{D_L}\right)^n \qquad (3)$$

D_H and D_L are the heavy and light isotopologues, respectively. The exponent n varies from zero in flow under completely turbulent conditions to one in purely diffusional regimes (Gonfiantini et al., 2018; Horita & Wesolowski, 1994).

For evaporation in the crusher device, we used equilibrium fractionation factors at 120°C calculated with the relationships presented by Horita & Wesolowski (1994), and a value for relative humidity that corresponds to the typical humid backgrounds set by the humidity generator ($h \approx 1\ \%$ for 10,000 to 14,000 ppmv of H_2O at 120°C). The diffusion fractionation factor was calculated with the molecular diffusivities of Merlivat (1978), and a value of n reflective of evaporation dominated by molecular diffusion (n=1), as expected for evaporation from porous materials like soil or leaf waters (Gonfiantini et al., 2018; Horita et al., 2008). Isotope ratios of the water vapor in air and the initial liquid (^{18}R and ^{2}R) were calculated with

the isotopic composition of the water background using a laboratory standard (DI2; $\delta^{18}O$ = -7.63 ± 0.06 and $\delta^{2}H$ = -50.72 ± 0.5) and with the average isotopic composition of the fluid inclusion data ($\delta^{18}O$ = -7.7 and $\delta^{2}H$ = -48.1), respectively.

For evaporation in the cave system, we used equilibrium fractionation factors at 25°C (Horita and Wesolowski 1994). The isotope ratios of the initial liquid were approximated with the average isotopic composition of the fluid inclusion data, and the isotope ratios of the cave air vapor were assumed to be equal to the isotope ratios of vapor in isotopic equilibrium with the initial liquid. Even though measured cave humidity in Borneo has always been close to 100%, we used a range in relative humidity of 60 to 90% to include the possibility of less humid conditions. Appropriate values of the n parameter for typical cave conditions are difficult to assign as they are not known. In laboratory experiments, however, high n values (close to 1) are obtained when evaporation rates are slow under quiet atmospheres (Gonfiantini et al., 2018). These conditions are likely similar to those experienced inside caves with poor ventilation. Similarly, n values close to 1 are expected if evaporation occurs in the epikarst where water evaporates through fractures and/or internal porosity. On the other hand, lower n values (close to 0.5) are observed in experiments when evaporation proceeds in open air conditions (Gonfiantini et al., 2018). These values may be more appropriate for caves with strong ventilation. Given these uncertainties, we use a range of n values of 0.5 to 1, which encompasses the full range of possible conditions that may occur in a cave system.

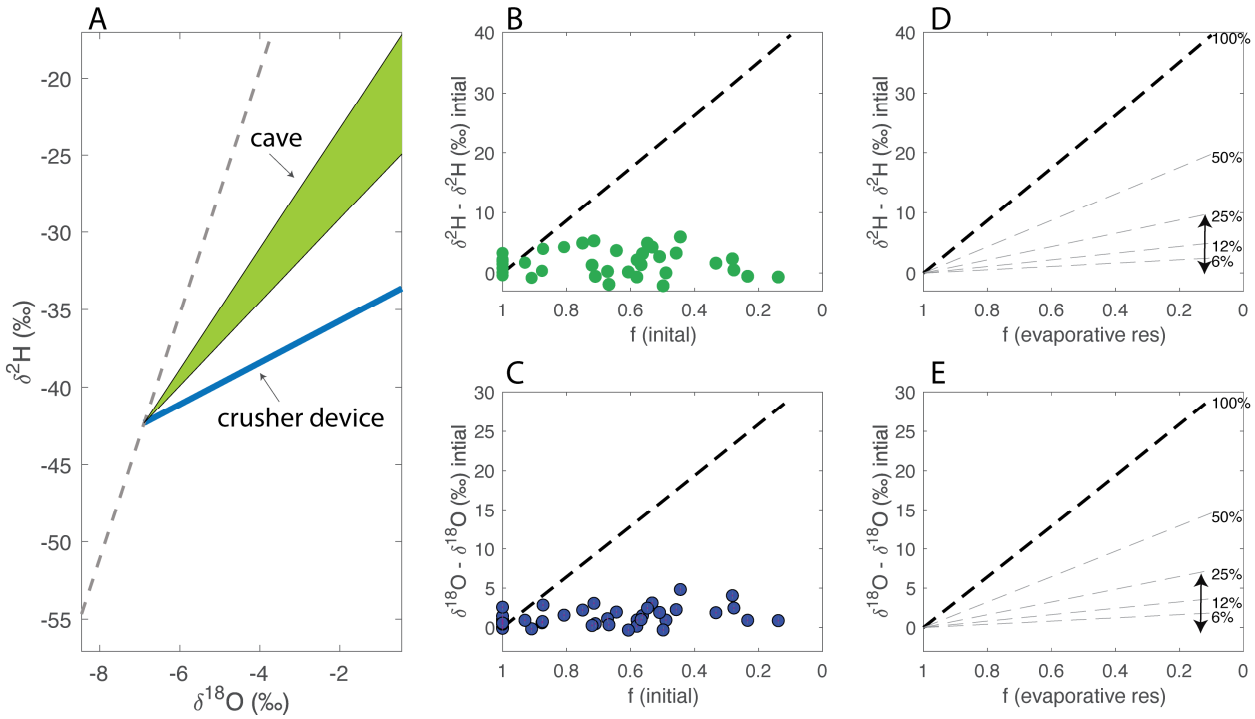

Figure 6. Results of the Rayleigh models for an evaporation process. A) Slopes in $\delta^{18}O$ vs. $\delta^{2}H$ space for evaporation in the crusher device (slope 1.4 - blue line) and range of slopes for evaporation in a cave (slopes 3.9 to 2.7 - green filled area). Dashed line is the LWML. B and C) Change in fluid inclusion $\delta^{18}O$ and $\delta^{2}H$ values,

respectively, vs. total water lost to evaporation (f = fraction of initial water remaining). Blue and green circles are $\delta^{18}O$ and $\delta^{2}H$ replicate analyses, respectively. F (initial) was calculated assuming that the initial water content for each sample is equal to that observed in the replicate analyses that plot closer to the LWML. D and E) Change in $\delta^{18}O$ and $\delta^{2}H$ values vs. water lost in an evaporative reservoir. Dashed lines indicate the trends predicted given different amounts of inclusions that experience evaporation (i.e., 100% means that all inclusions experience evaporation, and 25% means that only 1/4 of total inclusions loose water).

For evaporation in the crusher, the Rayleigh model predicts a slope of 1.4 (Fig. 6A, blue line). This value is statistically indistinguishable to the mean evaporative slope calculated with the replicate dataset (1 ± 0.6 2SE). This fact adds additional support to our interpretation that isotopic enrichments are the result of partial evaporation during analyses. For evaporation in the cave system, the model predicts slopes that are larger than the empirical estimate, ranging between 2.7 to 3.9 (Fig. 6A, red area), and where magnitudes are primarily controlled by the value of the n parameter (Supplemental 6). These results are generally consistent with the isotopic enrichments inferred for evaporation in cave systems. Values of evaporative slopes are not always reported, but two estimates are available. Warken et al. (2021) report a slope of 2.4 for fluid inclusion data from a stalagmite from Puerto Rico, and interpret it as the result of evaporation on top of the stalagmite. An additional slope of 3.9 was reported by Wortham et al. (2022), who interpreted it as the result of evaporation in the soil, epikarst or inside the cave. At face value, these slopes are consistent with the results of the model. Moreover, and in contrast to our Borneo stalagmite, evaporation is actually possible in both previously analyzed caves, as they experience seasonal changes in cave ventilation and humidity lower than 100 %. However, we caution that evaporative slopes were calculated from samples that are not coeval. Evaporative slopes may therefore be uncertain if the primary isotopic composition of the unevaporated water was variable. Moreover, evaporative loss through analyses cannot be ruled out, so results may incorporate modifications by both processes.

The results of both model scenarios predict larger fractionations – and thus larger distances from the LMWL – in samples that experienced more evaporation (Fig. 6B and 6C). Our observations from the replicate measurements are mainly consistent with these predictions. For example, in the replicate dataset there is a general relationship between lower water contents and larger $\delta^{18}O$ offsets from the LMWL (Figure 3B). Note that this is only true in 9 out of the 11 samples that we tested. Two samples show either no trend or a trend in the opposite direction (red dashed lines in Figure 3B), which cannot be explained by evaporative fractionation. However, we interpret these discrepancies as the result analytical errors in $\delta^{18}O$, variable water contents, difficulties in measuring strictly coeval samples, and variability in the number of inclusions that experience partial vs. total leakage. These are further discussed below (Sec. 4.3).

Although the model for the crusher device explains well the slopes of the evaporation trends, and the general relationship observed between distance from the LMWL and water loss, it does not correctly predict the magnitudes of the fractionations that we observe. For example, $\delta^{18}O$ and $\delta^{2}H$ enrichments in the model are more than 30 ‰ larger than our observations (Figure 6B and 6C). Smaller observed fractionations, though, can be explained by mixtures of water from pristine and partly leaked inclusions. While all inclusions become stretched upon

heating to 120 ˚C, only some of them start leaking, i.e. connect to the sample surface via cracks, crystal boundaries and interconnected pores and lose all or part of their water through evaporation. Inclusions that do not leak, preserve the original drip water isotopic composition. When these are crushed, the pristine water mixes with waters from partially evaporated reservoirs, and the magnitude of total observed fractionation is reduced. These mixing effects can be easily incorporated into the evaporation model, but direct comparison between predictions and our data are not straightforward. The main reason is that we do not know the relative size of the pool of inclusions in our samples that are amenable to leakage. Nevertheless, we can show that the range of observed fractionations are consistent with mixtures of 95 to 75% of pristine inclusions and 5 to 25% evaporated reservoirs (Figure 6D and 6E). It is important to note that this does not necessarily mean that only a small percentage of inclusions lost water; on the contrary, in some cases the majority of water was probably lost. For instance, we observe a range of more than 80% in the water content of some samples (Figure 6B and 6C). Part of that range likely results from variable initial water contents, but a considerable part of it is probably due to leakage and complete loss of water from inclusions through evaporation. Since completely evaporated reservoirs do not affect the measured isotopic composition, they can explain large variabilities in recovered water with only small concomitant changes in delta values.

4.3 Fluid inclusions, water contents, and isotopic modifications

The majority of early deglacial and glacial samples yield $\delta^{18}O$ values that fall close to the LMWL. The opposite is true for Holocene and late deglacial samples; most of them yield $\delta^{18}O$ values that plot to the right of the LMWL. We have demonstrated that isotopic enrichments can be explained by evaporative fractionations during analyses. Since we observe a close correlation between fractionations and the age of the samples, an open question is what features make some samples more amenable to isotopic modifications in the crusher device? The most striking differences between younger and older portions of the stalagmite are the size distributions of the fluid inclusions. While very large and elongated inter-crystalline inclusions are present throughout the stalagmite, the older parts have abundant and relatively large fluid inclusions that are orders of magnitude larger than the very small fluid inclusions observed in the Holocene and late deglacial portions of the stalagmite (see section 3.1). These observations explain why more water was recovered from older samples but the water content of the samples alone does not explain why the younger samples tend to show larger isotopic modifications.

Our hypothesis to explain why that occurs is that the very large and elongated inter-crystalline fluid inclusions (present throughout the stalagmite) are more likely to leak and lose water than other inclusions in the calcite fabric. A possible reason is the length of these elongated inclusions and their position between crystal boundaries, which gives them a better opportunity to be connected to the surfaces of the samples via cracks and interconnected pores. These inclusions, thus, form a partially evaporated reservoir that mixes with a more pristine reservoir from the other inclusions when the samples are crushed. Younger samples show larger isotopic modifications because the very small inclusions (pristine) likely contribute

only small amounts of water, and a relatively large fraction of water that was measured in these samples was provided by large, partially evaporated, inter-crystalline fluid inclusions. In the older samples, in contrast, where isotopic modifications are significantly smaller or absent, the inclusions that contribute to the pristine reservoir are orders of magnitude larger than those in the Holocene and late deglacial samples and likely provide most of the water. Although evaporation also occurs in these samples, the size of the partly evaporated reservoir relative to the pristine reservoir is much smaller. Given these observations, we suggest avoiding samples with low water contents and a large contrast of inclusion sizes. Figure 4B, however, illustrates that isotope compositions close to the LMWL are also possible with samples that contain only little water. That being said, we caution that additional observations from other stalagmites are necessary to draw broad conclusions on the leakage susceptibility of different fluid inclusions and on sampling strategies for fluid inclusion analyses.

4.4 Correction of evaporative trends

In this section we describe an approach to correct fluid inclusion water isotope measurements for evaporative fractionation during analysis, and we discuss the reliability of the proposed correction algorithm. The most straightforward approach to correct the data is to use the $\delta^2H/\delta^{18}O$ slope of the evaporative trends. This is possible because all samples should share the same slope, as they were subjected to the same conditions during analyses (e.g., temperature, relative humidity, flow regimes). To correct the data, we constructed linear models for each replicate measurement using the evaporative slope that was estimated with the Raleigh distillation model ($\delta^2H/\delta^{18}O$ =1.4; Figure 6A). The original (pristine) isotope compositions were then determined by the points of intersection between the linear models and the LMWL. Corrected data are presented in Figure 7.

Unlike the raw fluid inclusion data (Figure 5), the corrected data are in very close agreement to the calculated SC02 dripwater isotope values (Figure 7A and 7B). For example, calculated and measured $\delta^{18}O$ and δ^2H values show the same trends throughout the length of the record, and measured SSC01 $\delta^{18}O$ and δ^2H values are within ± 95% CI of calculated values from SC02. Moreover, as expected – given the shallow slopes of the evaporative trends – the correction has a larger relative effect on $\delta^{18}O$ values than on δ^2H values. Much closer agreement is also found between the fluid-calcite $\delta^{18}O$ temperatures and SC02 microthermometry estimates when the former are calculated with the corrected $\delta^{18}O$ values (Figure 7C). Corrected values are all within ± 95% CI of the microthermometry estimates.

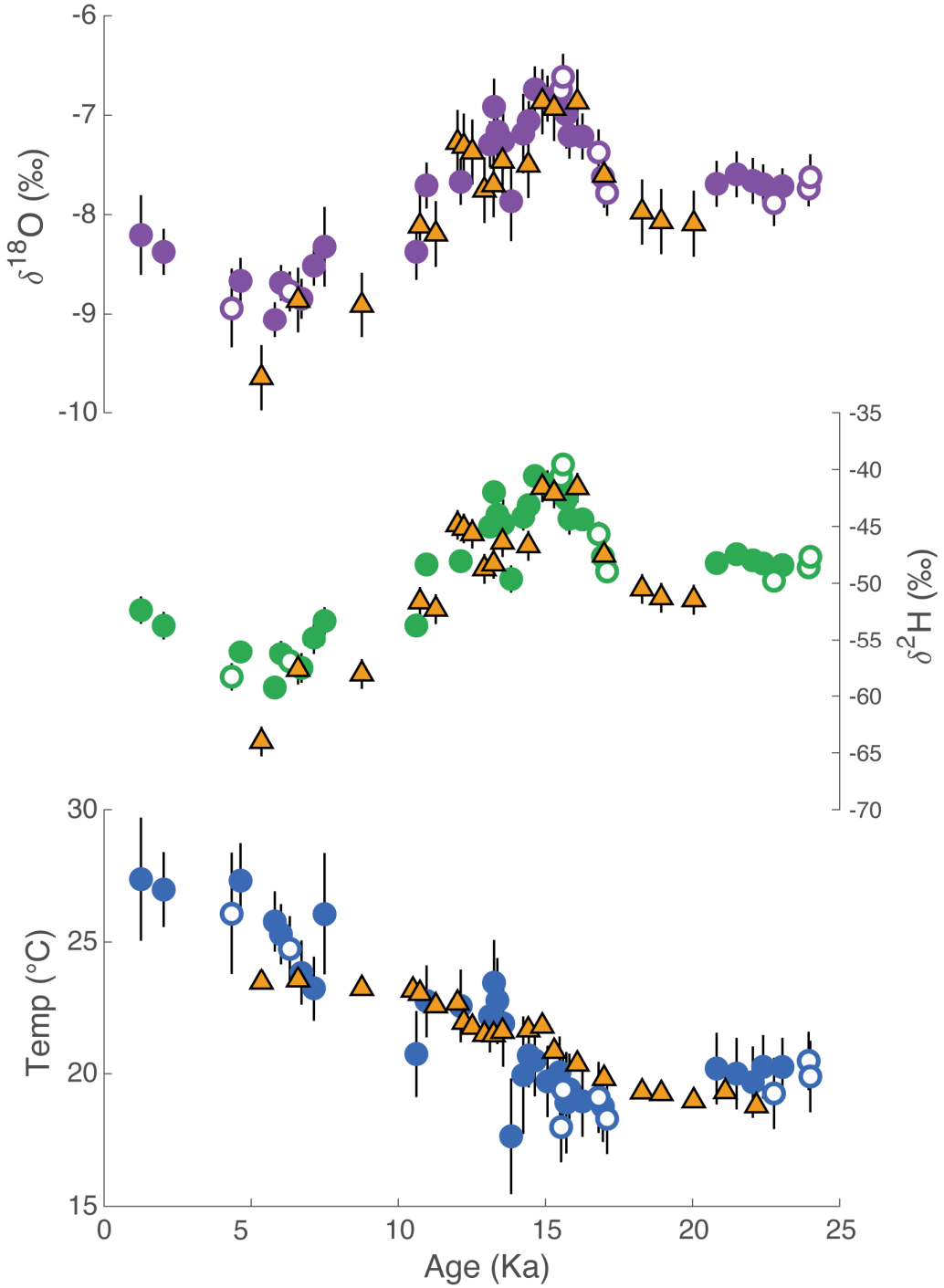

Figure 7. A) Corrected fluid inclusion $\delta^{18}O$ values of the SSC01 stalagmite (circles) and calculated drip water $\delta^{18}O$ values of the SC02 stalagmite (triangles). B) Corrected fluid inclusion $\delta^{2}H$ values of the SSC01 stalagmite (circles) and calculated drip water $\delta^{2}H$ values of the SC02 stalagmite with the LMWL triangles). C) fluid-calcite $\delta^{18}O$ temperatures of SSC01 from corrected $\delta^{18}O$ values (circles) and microthermometry temperatures of SC02 from Løland et al. (2022) (triangles). Fluid-calcite $\delta^{18}O$ temperatures were calculated with the Tremaine et al. (2011) relationship. Error bars are 68% confidence intervals. Open circles are samples that fell within 68% CI of the LMWL before correction.

We have shown that the correction procedure removes the disagreement between calculated and measured dripwater isotope values, and between fluid-calcite $\delta^{18}O$ temperatures and microthermometry estimates. However, our correction routine relies on independent knowledge of the LWML. We used the present-day LWML to correct data for analytical artifacts; however, in some settings the LMWL may not be precisely known or it may have been different in the past. For example, the LWML can vary because it depends on the deuterium excess of local precipitation, which is primarily controlled by the moisture conditions of the source regions (e.g., temperature, relative humidity and isotope composition; Pfahl & Sodemann, 2014), and the presence/absence of non-equilibrium processes during precipitation (e.g., re-moistening and rain drop evaporation; Lee & Fung, 2008; Martinelli et al., 1996). This is the main disadvantage of our correction routine, and it can be an important source of bias in paleoclimate reconstructions.

To examine the sensitivity of corrected values to possible changes in the LWML, we looked at results from the iTRACE experiment (He et al., 2021), which is a transient (20-11 ka) water isotope enabled simulation of global climate using the Community Earth System Model version 1.3. In the closest grid cell to the Borneo site, the model predicts variations in LMWL parameters of up to 3 ‰ in the intercept and 0.3 ‰ in the slope. The magnitude of these changes, however, are insufficient to impact corrected fluid inclusion data outside of analytical error (see Supplemental Figure 7). As an additional robustness check, we looked at LMWLs from three Global Network of Isotopes in Precipitation (GNIP) sites in the Indo-Pacific region. These sites are located at latitudes where seasonal migrations of the intertropical convergence zone (ITCZ) cause large differences in seasonal precipitation amounts. We use changes in LMWLs at these sites as proxies for hydrological conditions in Borneo during the deglaciation, where regional arid conditions are thought to be caused by a southward shift in the ITCZ over the Pacific (Buckingham et al., 2022; Carolin et al., 2013; Partin et al., 2007). We also find that changes in the LMWLs at these sites do not have an impact on data correction outside of analytical errors. These observations suggests that the correction is not very sensitive to changes in the LWML parameters within a realistic range (see Supplemental Figure 7).

4.5 Agreement between Borneo stalagmite paleothermometers

Our corrected fluid inclusion data presents an opportunity to test the performance of the empirical fluid-calcite $\delta^{18}O$ cave calibration of Tremaine et al. (2011). Empirical calibrations such as the one from Tremaine et al. (2011) are needed because speleothem calcite rarely forms in oxygen isotope equilibrium with dripwater (Guo & Zhou, 2019; Mickler et al., 2004). As previously discussed, fluid-calcite $\delta^{18}O$ temperatures determined with this cave calibration are statistically indistinguishable from independent microthermometry estimates over the length of both records (Figure 7C). Thus, the cave calibration of Tremaine et al. (2011) appears to perform very well in Borneo possibly because disequilibrium remained approximately constant through time. This is surprising given the evidence for changes in temperature and hydroclimate in Borneo through the deglaciation, which were likely accompanied by changes in the environmental variables that drive disequilibrium (e.g., PCP, cave air pCO2, drip rate, water

film thickness, and growth rates; e.g., Carlson et al., 2020; Deininger et al., 2021; Johnston et al., 2013). While counterintuitive at first sight, the observations can be explained if disequilibrium – at the timescales captured by our samples– is not very sensitive to changes in these variables. There is some evidence from theoretical models to support this idea. For example, Guo & Zhou (2019) recently published results of a reaction diffusion model that tracks the concentrations of isotopologues in the $CaCO_3$-DIC-H_2O system during speleothem formation. They found that their model is able to reproduce the temperature dependence of ^{18}O fractionations observed by Tremaine et al. (2011). Moreover, when environmental variables (PCP, cave air pCO_2, and water film thickness) are randomly varied by 25% in their model, the $\delta^{18}O$ value of calcite varies only by ± 0.23 ‰ (2σ). This corresponds to only ± 1.2 °C, a magnitude that cannot be detected given typical errors in fluid-calcite $\delta^{18}O$ temperatures. Thus, we hypothesize that disequilibrium in Borneo, despite changes in environmental variables that drive it, remained close to the average magnitudes observed in modern speleothems and within our error bars.

4.6 Deglacial hydroclimate evolution in Borneo

Corrected fluid inclusion data provide the first directly measured Borneo dripwater $\delta^{18}O$ and $\delta^{2}H$ values during the last deglaciation. These data agree well with previous estimates of hydrological conditions inferred from calcite $\delta^{18}O$ and with proxies for the strength of the Atlantic Ocean meridional overturning circulation (AMOC) (Figure 8). For instance, we observe a shift to the most positive dripwater $\delta^{18}O$ values during Heinrich event 1 (H-1), a time interpreted as a period of weakened regional convection based on stalagmite $\delta^{18}O$ measurements (Partin et al., 2007; Buckingham et al., (2022) and calculated dripwater $\delta^{18}O$ (Løland et al. 2022). Both the measured and calculated dripwater $\delta^{18}O$ records show a gradual decrease in dripwater $\delta^{18}O$ values during H-1, a small decrease during the Bølling-Allerød (BA), and a return to LGM values during the Early Holocene (Figure 8C and 8D). Especially for H-1, our data add new details to the existing dripwater $\delta^{18}O$ record, showing a late onset of the hydroclimate response when compared to the AMOC record, and even suggesting a two-step evolution. These features are worth further investigation.

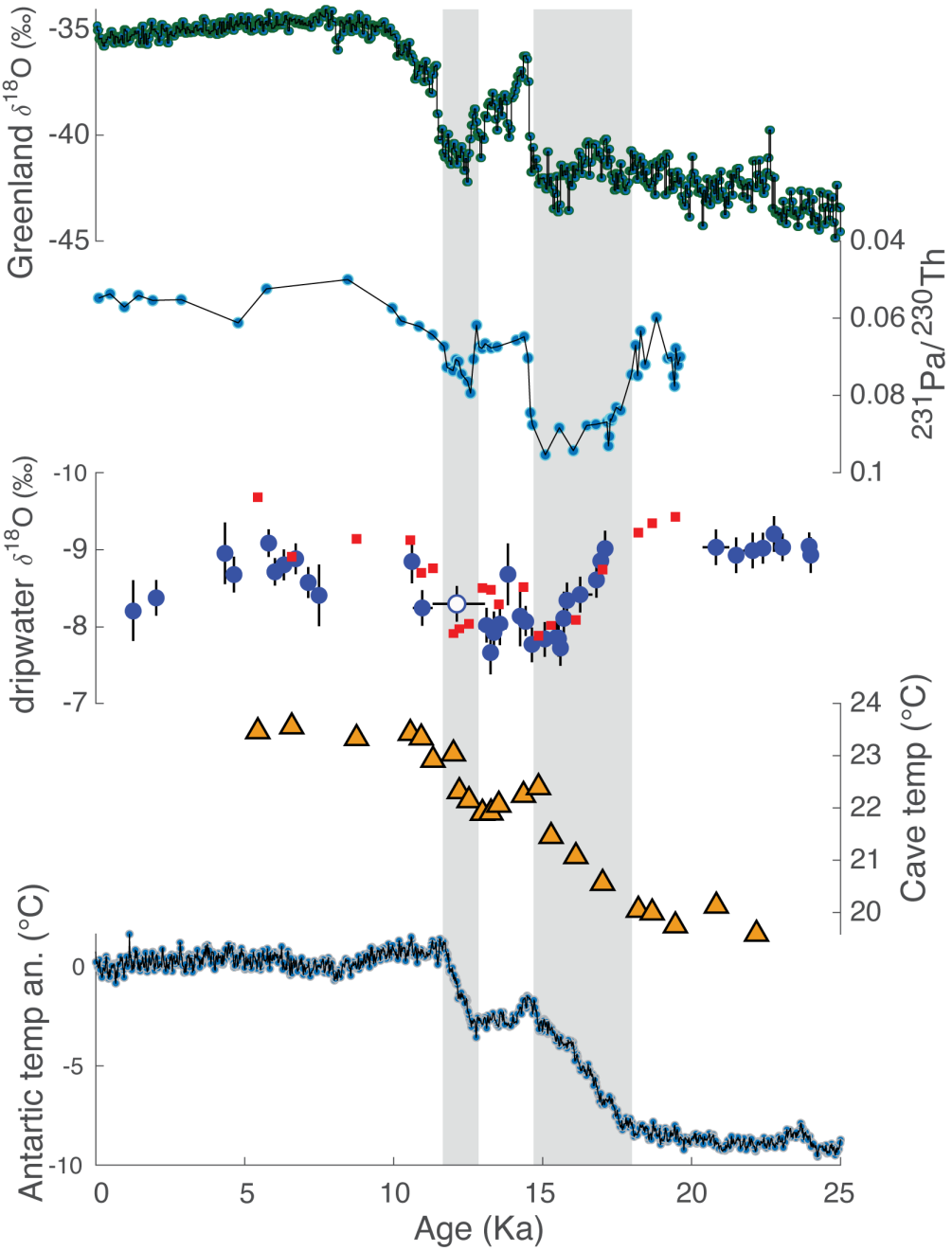

Figure 8. Comparison of Borneo dripwater $\delta^{18}O$ values with cave temperature and other paleoclimate records. A) Greenland ice core (NGRIP) $\delta^{18}O$, a proxy for Greenland temperature (North Greenland Ice Core Project members, 2004). B) Changes in North Atlantic Ocean meridional overturing circulation based on the $^{231}Pa/^{230}Th$ of N. Atlantic sediment core OCE326-GGC5 (McManus et al., 2004). C) Measured SSC01 fluid inclusion $\delta^{18}O$ values after correction for analytical artifacts (blue circles, errors bars are ± 69% ci), and calculated SC02 dripwater $\delta^{18}O$ values from (Løland et al., 2022) (red dots). Both data series were corrected for ice volume related changes the $\delta^{18}O$ value of the global ocean (see Løland et al., 2022 for details). The open blue symbol shows a sample that was obtained across a hiatus in SSC01 stalagmite, implying uncertainty in its age. D) SC02 cave temperatures from fluid inclusion microthermometry corrected for sea-level induced changes in cave altitude (Løland et al., 2022). E) Antarctic temperature anomaly (Parrenin et al., 2013).

5. Conclusions and recommendations

We measured the isotope composition of fluid inclusion waters in a stalagmite from Borneo that grew during the last deglaciation. We find that many samples ~~partially~~ lose water due to evaporation during warm-up before the crushing step, and that water loss and the magnitude of isotopic modifications are controlled by the type and size distribution of fluid inclusions. Partial evaporation results in $\delta^{18}O$ and $\delta^{2}H$ enrichments that follow typical evaporation lines with shallow $\delta^{18}O$/ $\delta^{2}H$ slopes. Through multiple replicate analyses of coeval samples, we constrain the mean value of the evaporative $\delta^{18}O$/ $\delta^{2}H$ slope at 1 ± 0.6 (2SE). This value is identical to the predictions of a Rayleigh distillation model that incorporates kinetic ^{2}H and ^{18}O fractionations during evaporation in the hot crushing apparatus.

We provide a robust and physically based method to correct for analytical modifications and demonstrate that it can be used to reliably correct data to pristine dripwater isotopic compositions. We find that corrected fluid-calcite $\delta^{18}O$ and resulting paleotemperatures show excellent agreement with independent dripwater $\delta^{18}O$ and temperature estimates, which implies only small variations in speleothem ^{18}O disequilibrium. The corrected data provide the first directly measured dripwater $\delta^{18}O$ and $\delta^{2}H$ estimates for Borneo across the last deglaciation and support the previously inferred hydroclimate evolution.

Our observations suggest that water loss during fluid inclusion water isotope analysis readily occurs and that the magnitude of isotopic modifications can vary from sample to sample. Future improvements to the analytical method should seek to remove these artifacts. In lieu of such improvements, we suggest that multiple replicate measurements of coeval samples and careful petrographic inspections be used to identify suitable samples, calcite fabrics, and the type of fluid inclusions that are prone to evaporative artifacts. Special attention should be given to samples with low water yields as these have been identified in this work and by others as samples that more likely show isotopic modifications. Caution is warranted when interpreting speleothem fluid inclusion isotope data that is not checked for or corrected for evaporation. This is especially true for $\delta^{18}O$ data as these are affected by non-equilibrium fractionation to a much greater extent than $\delta^{2}H$ relative to expected respective variations in precipitation.

6. Acknowledgments

This work was funded by the Norwegian Research Council (grant no. 262353/F20 to A.N.M.) and the European Research Council (grant no. 101001957 to A.N.M.). The analyses were performed at the Norwegian national infrastructure laboratory FARLAB (RCN grant no. 245907).

A.F. acknowledges support from Juan de la Cierva Fellowship (IJC2019040065-I) granted by the Spanish Ministry of Science and Innovation and co-funded by the European Development Fund and the European Social Fund. We thank Silvia Frisia for assistance with petrographic observations, Hege Kilhavn for helpful discussions, and Alena Dekhtyareva for assistance with relative humidity calculations. We also thank Judson Partin for assistance with the age model of SSC01, and Stacy Carolin for help with the iTrace model output.

7.0 Open Research

Data availability statement. Data archiving is currently underway in the EARTHCHEM archive. A temporary copy of the data is available as part of the supplementary information.

8.0 References

Affolter, S., Fleitmann, D., & Leuenberger, M. (2014). New online method for water isotope analysis of speleothem fluid inclusions using laser absorption spectroscopy (WS-CRDS). *Climate of the Past*, *10*(4), 1291–1304. https://doi.org/10.5194/cp-10-1291-2014

Affolter, Stéphane, Häuselmann, A., Fleitmann, D., Edwards, R. L., Cheng, H., & Leuenberger, M. (2019). Central Europe temperature constrained by speleothem fluid inclusion water isotopes over the past 14,000 years. *Science Advances*, *5*(6), eaav3809. https://doi.org/10.1126/sciadv.aav3809

Arienzo, M. M., Swart, P. K., Pourmand, A., Broad, K., Clement, A. C., Murphy, L. N., et al. (2015). Bahamian speleothem reveals temperature decrease associated with Heinrich stadials. *Earth and Planetary Science Letters*, *430*, 377–386. https://doi.org/10.1016/j.epsl.2015.08.035

Baker, A. J., Sodemann, H., Baldini, J. U. L., Breitenbach, S. F. M., Johnson, K. R., van Hunen, J., & Zhang, P. (2015). Seasonality of westerly moisture transport in the East Asian summer monsoon and its implications for interpreting precipitation δ^{18}O: EAST ASIAN RAINFALL

MOISTURE SOURCES. *Journal of Geophysical Research: Atmospheres*, *120*(12), 5850–5862. https://doi.org/10.1002/2014JD022919

van Breukelen, M. R., Vonhof, H. B., Hellstrom, J. C., Wester, W. C. G., & Kroon, D. (2008). Fossil dripwater in stalagmites reveals Holocene temperature and rainfall variation in Amazonia. *Earth and Planetary Science Letters*, *275*(1–2), 54–60. https://doi.org/10.1016/j.epsl.2008.07.060

Buckingham, F. L., Carolin, S. A., Partin, J. W., Adkins, J. F., Cobb, K. M., Day, C. C., et al. (2022). Termination 1 Millennial-Scale Rainfall Events Over the Sunda Shelf. *Geophysical Research Letters*, *49*(5). https://doi.org/10.1029/2021GL096937

Carlson, P. E., Noronha, A. L., Banner, J. L., Jenson, J. W., Moore, M. W., Partin, J. W., et al. (2020). Constraining speleothem oxygen isotope disequilibrium driven by rapid CO2 degassing and calcite precipitation: Insights from monitoring and modeling. *Geochimica et Cosmochimica Acta*, *284*, 222–238. https://doi.org/10.1016/j.gca.2020.06.012

Carolin, S. A., Cobb, K. M., Adkins, J. F., Clark, B., Conroy, J. L., Lejau, S., et al. (2013). Varied Response of Western Pacific Hydrology to Climate Forcings over the Last Glacial Period. *Science*, *340*(6140), 1564–1566. https://doi.org/10.1126/science.1233797

Craig H. (1961). Isotopic Variations in Meteoric Waters. *Science*, (133), 1702–1703. https://doi.org/DOI: 10.1126/science.133.3465.1702

Craig H & Gordon, L. I. (1965). Deuterium and oxygen 18 variations in the ocean and the marine atmosphere. In Tongiogi, E., V. & Lishi E F. (Eds.), *Proc. Stable Isotopes in Oceanographic Studies and Paleotemperatures* (pp. 9–130). Spoleto, Italy.

Dassié, E. P., Genty, D., Noret, A., Mangenot, X., Massault, M., Lebas, N., et al. (2018). A Newly Designed Analytical Line to Examine Fluid Inclusion Isotopic Compositions in a Variety of Carbonate Samples. *Geochemistry, Geophysics, Geosystems*, *19*(4), 1107–1122. https://doi.org/10.1002/2017GC007289

Deininger, M., Hansen, M., Fohlmeister, J., Schröder-Ritzrau, A., Burstyn, Y., & Scholz, D. (2021). Are oxygen isotope fractionation factors between calcite and water derived from speleothems systematically biased due to prior calcite precipitation (PCP)? *Geochimica et Cosmochimica Acta*, *305*, 212–227. https://doi.org/10.1016/j.gca.2021.03.026

Demény, A., Czuppon, G., Kern, Z., Leél-Őssy, S., Németh, A., Szabó, M., et al. (2016). Recrystallization-induced oxygen isotope changes in inclusion-hosted water of speleothems – Paleoclimatological implications. *Quaternary International*, *415*, 25–32. https://doi.org/10.1016/j.quaint.2015.11.137

Ellis, S. A., Cobb, K. M., Moerman, J. W., Partin, J. W., Bennett, A. L., Malang, J., et al. (2020). Extended Cave Drip Water Time Series Captures the 2015–2016 El Niño in Northern Borneo. *Geophysical Research Letters*, *47*(5). https://doi.org/10.1029/2019GL086363

Fleitmann, D., Burns, S. J., Mudelsee, M., Neff, U., Kramers, J., Mangini, A., & Matter, A. (2003). Holocene Forcing of the Indian Monsoon Recorded in a Stalagmite from Southern Oman. *Science*, *300*(5626), 1737–1739. https://doi.org/10.1126/science.1083130

Gonfiantini, R., Wassenaar, L. I., Araguas-Araguas, L., & Aggarwal, P. K. (2018). A unified Craig-Gordon isotope model of stable hydrogen and oxygen isotope fractionation during fresh or saltwater evaporation. *Geochimica et Cosmochimica Acta*, *235*, 224–236. https://doi.org/10.1016/j.gca.2018.05.020

de Graaf, S., Vonhof, H. B., Weissbach, T., Wassenburg, J. A., Levy, E. J., Kluge, T., & Haug, G. H. (2020). A comparison of isotope ratio mass spectrometry and cavity ring-down spectroscopy techniques for isotope analysis of fluid inclusion water. *Rapid Communications in Mass Spectrometry*, *34*(16). https://doi.org/10.1002/rcm.8837

Guo, W., & Zhou, C. (2019). Patterns and controls of disequilibrium isotope effects in speleothems: Insights from an isotope-enabled diffusion-reaction model and implications for quantitative thermometry. *Geochimica et Cosmochimica Acta*, *267*, 196–226. https://doi.org/10.1016/j.gca.2019.07.028

He, C., Liu, Z., Otto-Bliesner, B. L., Brady, E. C., Zhu, C., Tomas, R., et al. (2021). Hydroclimate footprint of pan-Asian monsoon water isotope during the last deglaciation. *Science Advances*, *7*(4), eabe2611. https://doi.org/10.1126/sciadv.abe2611

Horita, J., & Wesolowski, D. J. (1994). Liquid-vapor fractionation of oxygen and hydrogen isotopes of water from the freezing to the critical temperature. *Geochimica et Cosmochimica Acta*, *58*(16), 3425–3437. https://doi.org/10.1016/0016-7037(94)90096-5

Horita, J., Rozanski, K., & Cohen, S. (2008). Isotope effects in the evaporation of water: a status report of the Craig–Gordon model. *Isotopes in Environmental and Health Studies*, *44*(1), 23–49. https://doi.org/10.1080/10256010801887174

Johnston, V. E., Borsato, A., Spötl, C., Frisia, S., & Miorandi, R. (2013). Stable isotopes in caves over altitudinal gradients: fractionation behaviour and inferences for speleothem sensitivity to climate change. *Climate of the Past*, *9*(1), 99–118. https://doi.org/10.5194/cp-9-99-2013

837 Juson Partin. (2008). *Stalagmite reconstructions of Western Tropical Pacific climate from the*
838 *Last Glacial Maximum to the present.* (Dissertation). Georgia Institute of Technology.
839 Krüger, Y., Marti, D., Staub, R. H., Fleitmann, D., & Frenz, M. (2011). Liquid–vapour
840 homogenisation of fluid inclusions in stalagmites: Evaluation of a new thermometer for
841 palaeoclimate research. *Chemical Geology*, *289*(1–2), 39–47.
842 https://doi.org/10.1016/j.chemgeo.2011.07.009
843 Lee, J.-E., & Fung, I. (2008). "Amount effect" of water isotopes and quantitative analysis of post-
844 condensation processes. *Hydrological Processes*, *22*(1), 1–8.
845 https://doi.org/10.1002/hyp.6637
846 Løland, M. H., Krüger, Y., Fernandez, A., Buckingham, F., Carolin, S. A., Sodemann, H., et al.
847 (2022). Evolution of tropical land temperature across the last glacial termination. *Nature*
848 *Communications*, *13*(1), 5158. https://doi.org/10.1038/s41467-022-32712-3
849 Martinelli, L. A., Victoria, R. L., Silveira Lobo Sternberg, L., Ribeiro, A., & Zacharias Moreira, M.
850 (1996). Using stable isotopes to determine sources of evaporated water to the
851 atmosphere in the Amazon basin. *Journal of Hydrology*, *183*(3–4), 191–204.
852 https://doi.org/10.1016/0022-1694(95)02974-5
853 Matthews, A., Affek, H. P., Ayalon, A., Vonhof, H. B., & Bar-Matthews, M. (2021). Eastern
854 Mediterranean climate change deduced from the Soreq Cave fluid inclusion stable
855 isotopes and carbonate clumped isotopes record of the last 160 ka. *Quaternary Science*
856 *Reviews*, *272*, 107223. https://doi.org/10.1016/j.quascirev.2021.107223
857 Meckler, A. N., Affolter, S., Dublyansky, Y. V., Krüger, Y., Vogel, N., Bernasconi, S. M., et al.
858 (2015). Glacial–interglacial temperature change in the tropical West Pacific: A

comparison of stalagmite-based paleo-thermometers. *Quaternary Science Reviews*, *127*, 90–116. https://doi.org/10.1016/j.quascirev.2015.06.015

Meckler, A. N., Vonhof, H., & Martínez-García, A. (2021). Temperature Reconstructions Using Speleothems. *Elements*, *17*(2), 101–106. https://doi.org/10.2138/gselements.17.2.101

Merlivat, L. (1978). Molecular diffusivities of H2 160, HD160, and H2180 in gases, *69*, 9.

Mickler, P. J., Banner, J. L., Stern, L., Asmerom, Y., Edwards, R. L., & Ito, E. (2004). Stable isotope variations in modern tropical speleothems: Evaluating equilibrium vs. kinetic isotope effects. *Geochimica et Cosmochimica Acta*, *68*(21), 4381–4393. https://doi.org/10.1016/j.gca.2004.02.012

Millo, C. (2017). Last glacial and Holocene stable isotope record of fossil dripwater from subtropical Brazil based on analysis of fluid inclusions in stalagmites. *Chemical Geology*, 13.

Moerman, J. W., Cobb, K. M., Partin, J. W., Meckler, A. N., Carolin, S. A., Adkins, J. F., et al. (2014). Transformation of ENSO-related rainwater to dripwater δ^{18}O variability by vadose water mixing: ENSO variability in dripwater d18O. *Geophysical Research Letters*, *41*(22), 7907–7915. https://doi.org/10.1002/2014GL061696

Nehme, C., Kluge, T., Verheyden, S., Nader, F., Charalambidou, I., Weissbach, T., et al. (2020). Speleothem record from Pentadactylos cave (Cyprus): new insights into climatic variations during MIS 6 and MIS 5 in the Eastern Mediterranean. *Quaternary Science Reviews*, *250*, 106663. https://doi.org/10.1016/j.quascirev.2020.106663

879 North Greenland Ice Core Project members. (2004). High-resolution record of Northern
880 Hemisphere climate extending into the last interglacial period. *Nature*, *431*(7005), 147–
881 151. https://doi.org/10.1038/nature02805
882 Parrenin, F., Masson-Delmotte, V., Köhler, P., Raynaud, D., Paillard, D., Schwander, J., et al.
883 (2013). Synchronous Change of Atmospheric CO2 and Antarctic Temperature During the
884 Last Deglacial Warming. *Science*, *339*(6123), 1060–1063.
885 https://doi.org/10.1126/science.1226368
886 Partin, J. W., Cobb, K. M., Adkins, J. F., Clark, B., & Fernandez, D. P. (2007). Millennial-scale
887 trends in west Pacific warm pool hydrology since the Last Glacial Maximum. *Nature*,
888 *449*(7161), 452–455. https://doi.org/10.1038/nature06164
889 Pfahl, S., & Sodemann, H. (2014). What controls deuterium excess in global precipitation?
890 *Climate of the Past*, *10*(2), 771–781. https://doi.org/10.5194/cp-10-771-2014
891 Rogerson, M., Dublyansky, Y., Hoffmann, D. L., Luetscher, M., Töchterle, P., & Spötl, C. (2019).
892 Enhanced Mediterranean water cycle explains increased humidity during MIS 3 in North
893 Africa. *Climate of the Past*, *15*(5), 1757–1769. https://doi.org/10.5194/cp-15-1757-2019
894 Sodemann, H., Dekhtyareva A., Fernandez A., Seidl A., Zannoni D., Maccali J. (in preparation). A
895 flexible and precise calibration system for water vapour isotope CRDS applications.
896 Therese Weißbach. (2020). *Spectroscopic isotope ratio analysis on speleothem fluid inclusions -*
897 *analytics and paleoclimatic case studies* (Dissertation). Heidelberg University,
898 Heidelberg, Germany.
899 Tremaine, D. M., Froelich, P. N., & Wang, Y. (2011). Speleothem calcite farmed in situ: Modern
900 calibration of δ18O and δ13C paleoclimate proxies in a continuously-monitored natural

cave system. *Geochimica et Cosmochimica Acta*, *75*(17), 4929–4950. https://doi.org/10.1016/j.gca.2011.06.005

Uemura, R., Kina, Y., Shen, C.-C., & Omine, K. (2020). Experimental evaluation of oxygen isotopic exchange between inclusion water and host calcite in speleothems. *Climate of the Past*, *16*(1), 17–27. https://doi.org/10.5194/cp-16-17-2020

Wang, Y. J., Cheng, H., Edwards, R. L., An, Z. S., Wu, J. Y., Shen, C.-C., & Dorale, J. A. (2001). A High-Resolution Absolute-Dated Late Pleistocene Monsoon Record from Hulu Cave, China. *Science*, *294*(5550), 2345–2348. https://doi.org/10.1126/science.1064618

Warken, S. F., Weißbach, T., Kluge, T., Vonhof, H., Scholz, D., Vieten, R., et al. (2022). Last glacial millennial-scale hydro-climate and temperature changes in Puerto Rico constrained by speleothem fluid inclusion d18O and d2H values. *Climate of the Past*, *18*(1), 167–181. https://doi.org/10.5194/cp-18-167-2022

Weng, Y., Touzeau, A., & Sodemann, H. (2020). Correcting the impact of the isotope composition on the mixing ratio dependency of water vapour isotope measurements with cavity ring-down spectrometers. *Atmospheric Measurement Techniques*, *13*(6), 3167–3190. https://doi.org/10.5194/amt-13-3167-2020

Wortham, B. E., Montañez, I. P., Swart, P. K., Vonhof, H., & Tabor, C. (2022). Variability in effective moisture inferred from inclusion fluid δ18O and δ2H values in a central Sierra Nevada stalagmite (CA). *Quaternary Science Reviews*, *279*, 107399. https://doi.org/10.1016/j.quascirev.2022.107399

York, D., Evensen, N. M., Martínez, M. L., & De Basabe Delgado, J. (2004). Unified equations for the slope, intercept, and standard errors of the best straight line. *American Journal of Physics*, *72*(3), 367–375. https://doi.org/10.1119/1.1632486